VI International Conference on Particle-based Methods – Fundamentals and Applications
PARTICLES 2019
E. Oñate, M. Bischoff, D.R.J. Owen P. Wriggers, , & T. Zohdi (Eds)

ROLE OF SLIDING CONTACTS IN SHEAR BANDING AFFECTING GRANULAR MATERIALS

J. LIU[1], F. NICOT[2], A. WAUTIER[3] AND W. ZHOU[1]

[1] State Key Laboratory of Water Resources and Hydropower Engineering Science
Wuhan University
299 Bayi Road, 430072 Wuhan, China
e-mail: liujy@whu.edu.cn (Jiaying Liu) ; zw_mxx@whu.edu.cn (Wei Zhou)

[2] ETNA, IRSTEA
Université Grenoble Alpes
Domaine Universitaire, 38402 Saint Martin d'Hères, France
e-mail: francois.nicot@irstea.fr

[3] Aix-Marseille University, IRSTEA, UR RECOVER
3275 Rte Cézanne, CS 40061, 13182 Aix-en-Provence Cedex 5, France
e-mail: antoine.wautier@irstea.fr

Key words: granular materials, DEM, contact sliding, meso-structures, shear banding

Abstract. Shear banding is a widely concerned issue caused by shearing in the field of granular geomechanics. At the macroscopic scale, the constitutive models meet difficulties to describe how and why the shear band forms within the discrete granular assembly. The contact network inside the overall granular assembly helps us to understand the origin of some macroscopic features. Between contacting particles, sliding can occur, which is associated with the plastic dissipation. This local contact sliding may induce the rearrangement of local structures, and then contribute to the macroscopic failure characterized by larger patterns, such as shear banding. In this paper, we conduct DEM simulations using a dense specimen, and during the loading process an evident shear band appears. Then the contact sliding ratio, sliding index, and the relationship between the contact sliding and the mesostructural changes are investigated. Main conclusions are: sliding contacts firstly distribute randomly within the granular assembly, and will concentrate within the shear band after the stress peak; the sliding ratio and the sliding index show different evolution trend and distribution properties; sliding contacts are not within the strong contact network when the threshold to distinguish the strong and weak network is proper, but will be strongly influenced by the force chain buckling; considering the relation between the sliding and the meso loop exchanges, the topological dilations are related to the higher probability of contact sliding and plastic dissipation.

1 INTRODUCTION

Granular materials are quite common and simple in nature and they have been widely utilized as construction materials in the field of civil engineering. Then the mechanical

behaviours of granular materials have attracted much attention among engineers and researchers. For decades, the shear banding problem in frictional granular materials has been concerned, which contains a number of challenges in mathematical description and constitutive modelling [1,2]. Many publications incorporate micromechanical features, such as contact fabric, particle rolling and contact sliding, to reveal the original mechanism of shear banding [3-6].

Microscopic features could be related to some macroscopic evolutions in granular materials. For example, the stress-force-fabric (SFF) relationship has built the direct links between micro contact forces and macro stress quantity [7-11]. Considering the contacts and particles at the microscale, the sliding between particles may occur when the Mohr-Coulomb criterion is fulfilled. The microscopic failure, or microscopic shear behaviours, should contribute to the macroscopic shear failures such as shear banding.

The discrete numerical simulation has been widely applied in simulating the multiscale behaviours of granular media, owing to its simplicity of obtaining the microscopic information and the reasonable accordance of macroscopic responses to laboratory tests. Classical Discrete Element Method (DEM) has been adopted in investigating the strain localization for granular materials [12-14]. Besides, the modified or combined methods for DEM are capable to investigate the influences of the irregular shape and particle breakage on the shear banding [15,16]. For DEM simulations, the contact sliding is the unique mechanism in plastic energy dissipation. How the sliding contacts distribute and evolve should affect the mesostructural rearrangements in granular assemblies. Since the strong contact network (usually selected using the average normal contact ratio [17,18]) and the mesostructural topology (in 2D, loop structures are important [19-21]) are important characterizations in granular materials, the relationship between the contact sliding and them should also been further considered.

In this paper, we focus on the micro- and mesoscopic evolutions in granular materials during the shear band forming. Investigations are based on the quasi-2D biaxial DEM simulations (with a single layer of 3D particles), under the same loading conditions as our previous work [22]. The evolution and distribution of the contact sliding ratio and the sliding index are considered, and the sliding behaviours within the strong contact network as well as the topological changes are explored to identify the specific roles of sliding in shear banding.

2 DEM SIMULATION AND SHEAR BANDING

2.1 Parameters and models of DEM

We use the Discrete Element Method (DEM) proposed by Cundall and Strack [23] for the numerical simulations, based on the open-source software YADE [24]. The simple linear contact model is adopted, in which the normal and tangential contact forces (F_n and F_t) are computed as follows:

$$\begin{cases} F_n = k_n \delta_n, \\ dF_t = k_t d\delta_t, \quad F_t \le F_n tan\phi \end{cases} \tag{1}$$

where k_n, k_t are the normal and tangential stiffness respectively, δ_n, δ_t are the corresponding relative displacements in normal and tangential direction, and ϕ is the friction angle which is a threshold limiting the relative sliding between particles. Relative sliding behaviour between spheres in a contact will take place when the tangential contact force reaches the maximum

value, as described by Eq. (1).

The quasi-2D biaxial test using DEM is carried out to model the mechanical behaviours and the shear band formation. The numerical simulation is conducted by using a model containing a single layer of 20,000 spheres within a rectangle domain, as shown in Fig. 1. The particle sizes obey a uniform distribution with average radii $D_{50} = 0.008\text{m}$ and $d_{max}/d_{min} = 2$. To create the sample, particles are randomly generated within the domain and their sizes are growing to reach the final isotropic state under a confining pressure of 100 kPa. The gravity is not considered, and the boundaries are set as rigid frictionless walls. The key parameters for the contact model: k_n/D_s is set to 300 MPa, where $D_s = R_1R_2/(R_1 + R_2)$; k_t/k_n is set to 0.5; the friction angle ϕ is 35°.

After confining, the numerical specimen reaches a relative dense state (initial porosity is 0.161). Then we apply the biaxial loading is applied, as shown in Fig. 1: the compression is imposed in the vertical direction (σ_{22} and ε_{22}) with a strain rate of the upper and lower walls equals to 0.01 /s. In the lateral direction (σ_{11} and ε_{11}), the pressure is maintained constant to 100 kPa. The stress and strain characterization are then described as follows: deviatoric stress $q = \sigma_{22} - \sigma_{11}$ and volumetric strain $\varepsilon_v = \varepsilon_{11} + \varepsilon_{22}$.

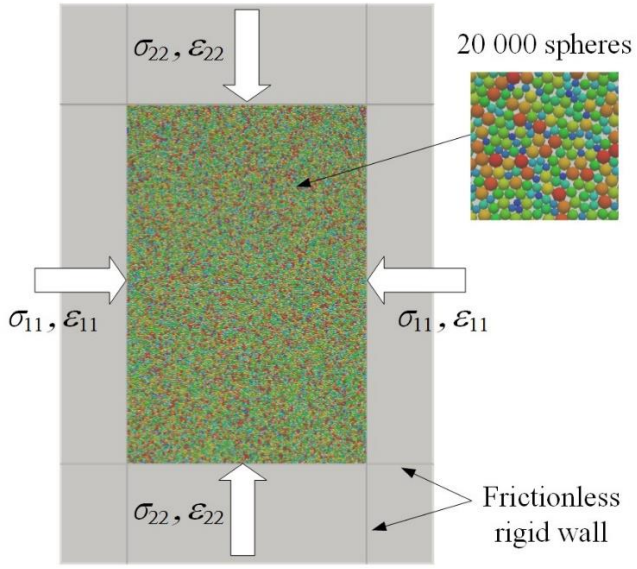

Figure 1: DEM model for biaxial tests

2.2 Macroscopic responses

Figure 2 gives the macroscopic evolutions of the deviatoric stress q and the volumetric strain ε_v. Similar to other publications [4,12,13], the deviatoric stress q experiences the hardening and the softening phases, while ε_v manifests a clear tendency of dilation. We select States from A to G, to track the evolution of the strain localization pattern and the macroscopic stress and strain features. The corresponding incremental deviatoric strain fields of the 7 states are shown in Fig. 3, demonstrating the evolution of local strain distribution pattern from homogeneity to heterogeneity in space. The Moran's Index can quantitatively capture the heterogeneity evolution, which was detailed explained in our previous work [22].

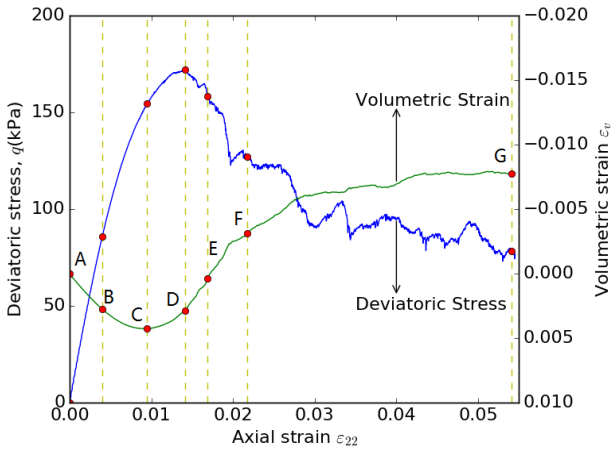

Figure 2: Strain softening process of dense specimen under biaxial test

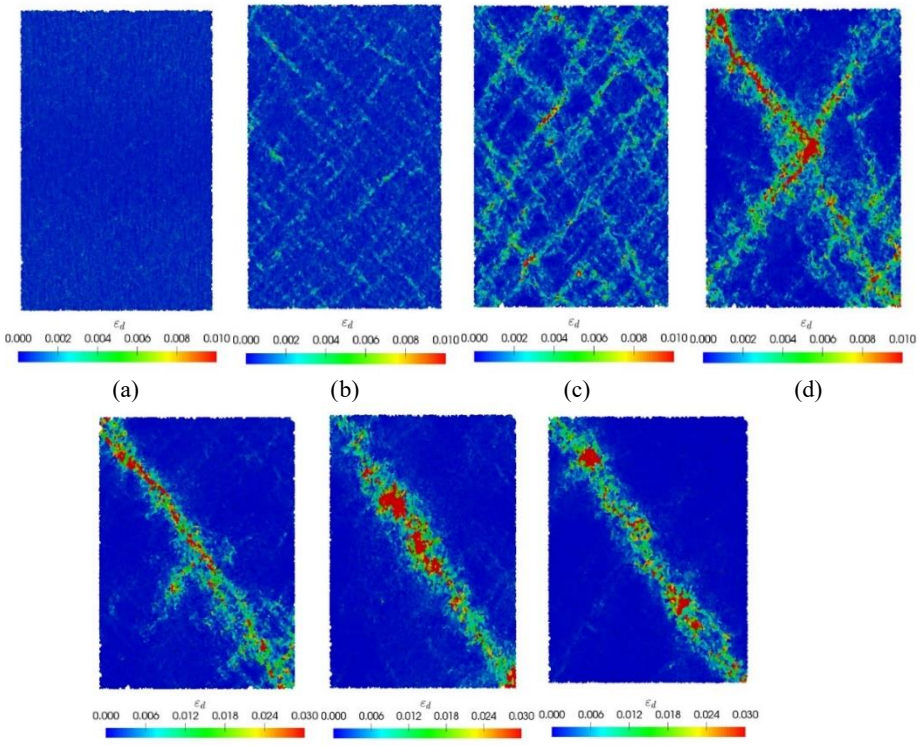

Figure 3: Spatial distributions of the incremental deviatoric strain for different loading states. (a) State A: ε_{22} = 0.0; (b) State B: ε_{22} = 0.0040; (c) State C: ε_{22} = 0.0095; (d) State D: ε_{22} = 0.0141; (e) State E: ε_{22} = 0.0169; (f) State F: ε_{22} = 0.0217; (g) State G: ε_{22} = 0.0541.

3 SLIDING CONTACTS AND RELATIVE MESO-STRUCTURES

3.1 Distribution of sliding contacts

Based on the framework of DEM, relative sliding behavior between connected spheres will take place when the tangential contact force reaches the maximum value, which is limited by

both the normal force and the friction angle, as described by Eq. (1). The sliding at one contact means the failure or dissipative mechanism at the microscopic scale. The ratio of sliding contacts, defined as $S_r = N_s/N_c$, can describe the proportion of microscopic failure for the granular assembly, in which N_s denotes the number of sliding contacts and N_c is the number of the total. The evolution of the ratio of sliding contacts is shown in Fig. 4, and S_r is divided into two parts (inside and outside the shear band, in these conditions N_s and N_c are considered for the corresponding domains) after the State E. At the beginning, the proportion of the sliding contacts rises gradually until the State C, which denotes that rearrangements of the bulk attains the maximum. After the peak value of the sliding ratio, the probability of sliding reduces gradually. When the single shear band ultimately appears, the sliding ratio stabilize, at the level about 0.007. During this period, the magnitudes of sliding ratios inside the shear band and outside the shear band manifest differently. The sliding contacts are mostly centralized within the shear band area, while only a small proportion of sliding contacts appear outside this area, which can be intuitively seen in Fig. 5 for States D and F.

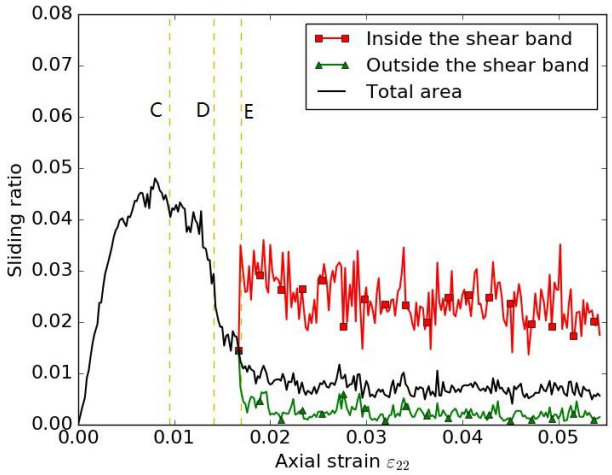

Figure 4: Evolution of the sliding ratio versus axial strain

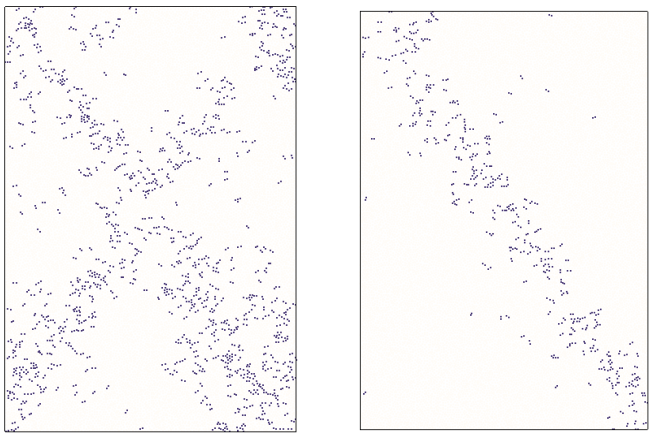

(a) (b)

Figure 5: Distribution of sliding contacts: (a) State D and (b) State F

To better describe the degree of frictional mobilization for all the contacts, not only the sliding ones, a sliding index Ip is defined as:

$$I_{\mathrm{p}} = \frac{F_t}{F_n \tan\phi} \tag{2}$$

When I_p is near to 1.0, the contact is prone to slide; on the contrary, when I_p is near to 0, the contact is regarded as quite stable. Figure 6 shows the evolution of the average sliding index during the biaxial loading process, with the separate curves for areas inside and outside the shear band after State E. Similar to the evolution of the sliding ratio in Fig. 5, the average I_p experiences an increase at the beginning, and then decreases to a steady value during the development of the final shear band. The peak value of the sliding index appears at State D, which is associated with the stress peak. The S_r peak comes earlier than the I_p peak. Indeed, it can be assumed that sliding contacts belong to discrete local failures, without propagating to the total area; however, the average I_p is considered for all the contacts within the assembly. Therefore, the overall responses of I_p can reflect the evolving tendency of the stress. After the peak, I_p declines a little with small discrepancies of the two domains when shear band forms.

Besides, the distribution of I_p is quite different from the distribution of S_r in space, as shown in Fig. 7(a). At State F, there exists a clear single shear band, however, the sliding ratio distribution in space does not show any strain localization patterns. Then, we choose another parameter, the incremental sliding index dI_p between steps. It can be calculated using the difference of the sliding index between the current step i and the previous step i-1, i.e. $\mathrm{d}I_p = {I_p}^{i} - {I_p}^{i-1}$. According to the definition, dI_p should fall in the range [-1, 1]. Positive values denote that the contact is nearer to the sliding, while negative values means that the contact is less possible to slide compared to the previous step. It can be seen that in Fig. 7(b), both large and small values of dI_p concentrate within the shear band area. That is to say, inside the shear band, large changes in contact state are involved, which can induce the quick and temporal rearrangements.

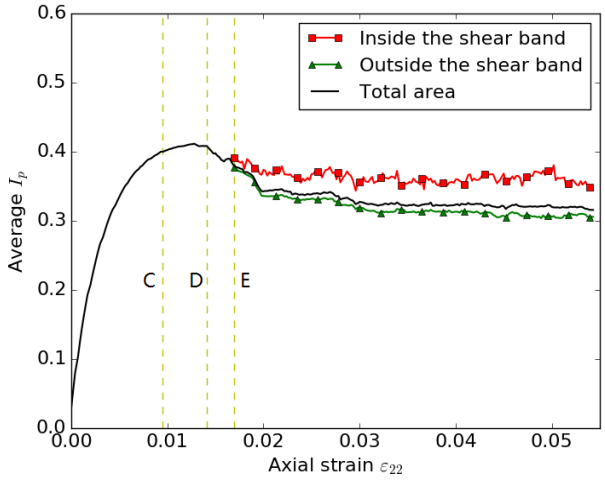

Figure 6: Evolution of average sliding index I_p

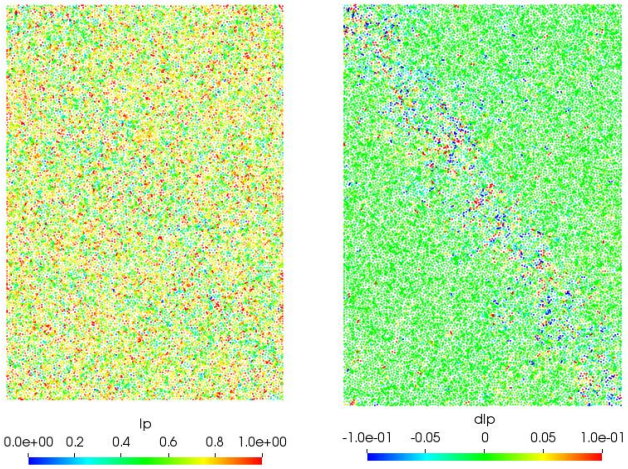

(a) (b)

Figure 7: Distributions of sliding index I_p (a) and incremental sliding index dI_p (b) within the granular sample at State F

3.2 Sliding contacts and strong contact network

The contact network within the granular assembly can be divided into the strong and weak phase using the contact force threshold [17,18]. In most cases, the average contact force is used as the threshold, and the strong contact subnetwork is regarded as the important force transmission path. By introducing assumptions such as the linear path and the particle number, force chain structures can be selected from the strong contact network [21,25].

In this paper, we consider the accurate and comprehensive effects of strong contact network, and the sets of contacts with forces larger than several given values are considered. The cutoff ζ, denoting the ratio to the average normal contact force, is used to identify the set S_ζ. Then S_ζ contains the contacts which undertake forces larger than ζf_0, where f_0 denotes the average contact force within the granular assembly.

Within the different strong contact networks distinguished by ζ, the sliding ratio diverges. Figure 8 show the evolution of sliding ratio S_r versus ζ for the 7 selected states. Almost all the curves in Fig. 8 reflect the fact that sliding contacts do not exist in the strong contact network when $\zeta > 1.5$. That is to say, the contact sliding as the microscopic failure, is excluded from the really strong contacts. As for the range $\zeta < 1.0$, the sliding ratio of State C owns the highest magnitude, which is corresponding to Fig. 4. Considering the unique features of sliding ratio of strong contact network of all states, possibly the better threshold for the strong and weak phase of the contact network should fall in $[1.0f_0, 1.5f_0]$.

Liu et al. [22] have defined the average sliding ratio S_{rp} around the particles, and based on this concept, they found that contact sliding is not directly relating to the force chain buckling, but will be influenced around the force chain buckling area. Since force chains are selected within the strong contact network when $\zeta = 1.0$, it can be assumed that the contact sliding has no intersection with the strong contact network, but the failure within the strong contact network may induce the sliding occurring and accumulating.

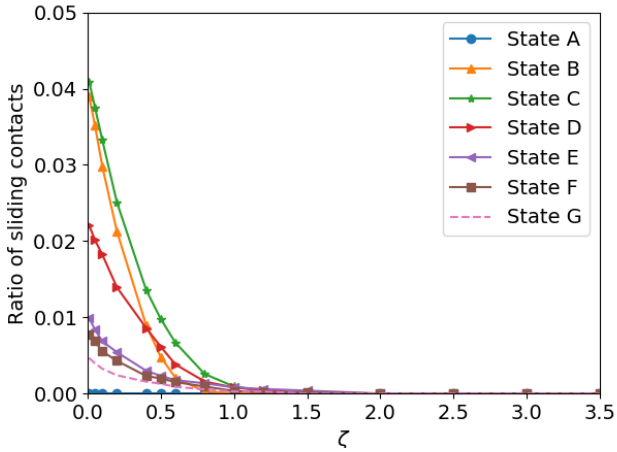

Figure 8: Sliding ratio within the strong contact network distinguished by ζ

3.3 Sliding contacts and loop transformation

The overall contact network of the granular assembly can be tessellated into meso loops, which are quite convenient to analyze the local deformation features in 2D granular materials [26,27]. From step to step, loops may keep constant or transform to other structures. The transformations or exchanges between local structures are temporal and complex, which will lead to the systematic change of the overall structure.

Loops within the granular assembly can be categorized by the number of particles of the circle. L6, denoting the cell connected by 6 spheres in 2D simulations, has been deeply investigated in many publications [12,19,21] for its capability of deformation. In this paper we take L6 as an example to explore the topological exchanges, and possible changes for L6 can be shown in Fig. 10. The change in next step, we call it “Future”, and we name 3 types of changes:

- Future_6C, for unchanged L6
- Future_6S, for L6 which will decompose to smaller ones
- Future_6L, for L6 which will change to a larger loop

The transformations and exchanges of loops are corresponding to the contact loss and gain within the contact network. Whether these changing contacts are sliding will indicate the plastic energy dissipation. Figure 9 give the average sliding ratio information for L6 with different futures respectively. Loops associated with changes, i.e. Future_6L and Future_6S, obtain higher sliding ratios than the constant ones during the biaxial loading. Furthermore, dilative loops (Future_6L) are more likely to involve a higher probability of sliding contacts and dissipating behaviors than the contractive ones (Future_6S) do.

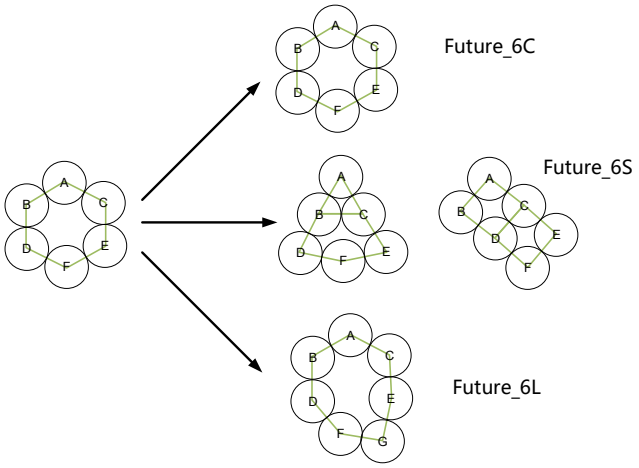

Figure 9: Possible changes for L6 loops between steps

Considering the average sliding ratios of L6 with different futures inside and outside the shear band, the dissipative behaviors could diverse, especially for the dilative changes. We can see that in Figure 11, loop exchanges within the shear band are associated with larger sliding ratios, especially for the dilative changes which reach the magnitude nearly 0.1. Even though there exist a few enlargements outside the shear band, the involving dissipation is not very obvious in comparison with the constant cells and the shrinkage ones inside the shear band.

Dilative loops at the mesoscopic scale should be related to the macroscopic dilatancy, which has been regarded as an irreversible plastic characteristic in soil mechanics [28][29]. The sliding ratio evolutions within the meso structures has revealed that the correlation between plastic energy dissipation and the dilatancy at the mesoscale. The contact sliding may not lead to the contact loss or gain, also the contact loss and gain may not involve plastic sliding behaviors. However, the sliding behaviors are easier to break the contacts and form larger local structures which lead to the dilatancy. The process should be irreversible, and once these kinds of behaviors accumulate and reach a high percentage, the plastic phase of the bulk appears. Shear banding is one kind of shear failures that local rearrangements concentrate within the localized area, and the dilative exchanges of loops should mainly occur within the banding zones.

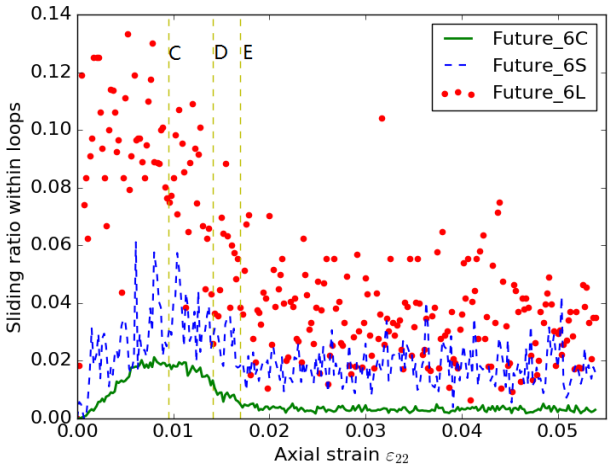

Figure 11: Sliding ratios within L6 for different futures

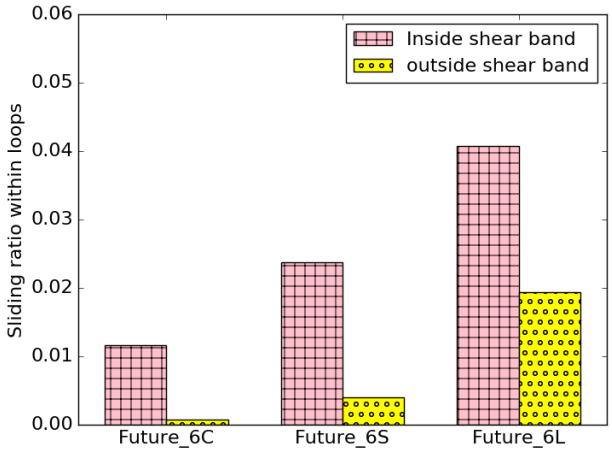

Figure 12: Sliding ratios of L6 with different futures in different domains

4 CONCLUSIONS

By conducting numerical DEM biaxial tests for a dense granular assembly, this paper investigates the contact sliding evolution and distribution within the specimen during shear banding, and identifies the relationships between the mesostructural changes and the contact sliding. Main conclusions are as follows:

- According to the spatial distribution of incremental shear strains of the dense granular assembly, it can be concluded that the heterogeneity develops gradually along the biaxial loading, until the final shear band forms. Inside the shear band, the sliding contacts, high values of incremental sliding index magnitude and loop exchanges are concentrated.
- Both the sliding ratio and sliding index demonstrate a peak in the evolution curves,

which is earlier or close to the macro stress peak. Furthermore the peak of sliding index could reflect the macro stress peak. By using different threshold to distinguish the strong and weak contact network, it is concluded that sliding contacts are located outside strong contact network and the threshold for the strong contact network may be 1 to 1.5 times average contact force.

- During the biaxial loading process, the loop type L6 could be constant, dilative or contractive in topology. The higher contact sliding ratio is associated with the dilative exchanges, which indicates that the plastic dissipation is quite essential to the dilatancy at the meso-scale.
- Thanks to this characterization of the microstructure features inside shear band domain, the present study paves the way for a deeper understanding of the micromechanical mechanisms responsible for the existence of shear bands in dense granular materials. The understanding of the link between contact sliding, mesostructure deformations and macroscopic shear banding and softening are now within reach.

REFERENCES

[1] Vardoulakis, I. and Graf, B. Calibration of constitutive models for granular materials using data from biaxial experiments. *Géotechnique* (1985) **35(3)** : 299-317.

[2] Borja, R. I. and Atilla A. Computational modeling of deformation bands in granular media. I. Geological and mathematical framework. *Comput. Method. Appl. Mech. Eng.* (2004) **193.27-29**: 2667-2698.

[3] Tordesillas, A. Force chain buckling, unjamming transitions and shear banding in dense granular assemblies. *Philos. Mag* (2007) **87.32**: 4987-5016.

[4] Zhou, B., Huang, R., Wang, H. and Wang, J. DEM investigation of particle anti-rotation effects on the micromechanical response of granular materials. *Granul. Matter* (2013)**15.3**: 315-326.

[5] Oda, M. and Kazuyoshi I. Study on couple stress and shear band development in granular media based on numerical simulation analyses. *Int. J. Eng. Sci* (2000)**38.15**: 1713-1740.

[6] Zhao, J. and Guo N. The interplay between anisotropy and strain localisation in granular soils: a multiscale insight. *Géotechnique* (2015)**65.8**: 642-656.

[7] Li, X. and Yu, H-S. On the stress–force–fabric relationship for granular materials. *Int. J. Solids. Struct* (2013)**50.9**: 1285-1302.

[8] Guo, N. and Zhao J. The signature of shear-induced anisotropy in granular media. *Comput. Geotech* (2013)**47**: 1-15.

[9] Bathurst, R.J. and Rothenburg, L. Observations on stress-force-fabric relationships in idealized granular materials. *Mech. Mater* (1990)**9.1**: 65-80.

[10] Kruyt, N. P. Micromechanical study of fabric evolution in quasi-static deformation of granular materials. *Mech. Mater* (2012)**44**: 120-129.

[11] Ouadfel, H. and Rothenburg, L. Stress–force–fabric'relationship for assemblies of ellipsoids. *Mech. Mater* (2001)**33.4**: 201-221.

[12] Zhu, H., Nguyen, H. N., Nicot, F. and Darve, F. On a common critical state in localized and diffuse failure modes. *J. Mech. Phys. Solids* **(2016)**95: 112-131.

[13] Gu, X., Huang M. and Qian J. Discrete element modeling of shear band in granular materials. *Theor. Appl. Fract. Mech* (2014) **72**: 37-49.

[14] Jiang, M. and Zhang W. DEM analyses of shear band in granular materials. *Eng. Computations* (2015)**32.4**: 985-1005.

[15] Zhou, W., Yang, L., Ma, G., Xu, K., Lai, Z. and Chang, X. DEM modeling of shear bands in crushable and irregularly shaped granular materials. *Granul. Matter* (2017)**19.2**: 25.

[16] Ma, G., Regueiro, R. A., Zhou, W., Wang, Q. and Liu, J. Role of particle crushing on particle kinematics and shear banding in granular materials. *Acta. Geotech* (2018)**13.3**: 601-618.

[17] Radjai, F., Stéphane R. and Moreau J. J. Contact forces in a granular packing. *Chaos: An*

Interdisciplinary Journal of Nonlinear Science (1999)**9.3**: 544-550.

[18] Voivret, C., Radjai, F., Delenne, J. Y. and El Youssoufi, M. S. Multiscale force networks in highly polydisperse granular media. *Phys. Rev. Lett* (2009)**102.17**: 178001.

[19] Zhu, H., François N. and Darve F. Meso-structure organization in two-dimensional granular materials along biaxial loading path. *Int. J. Solids. Struct* (2016) **96**: 25-37.

[20] Tordesillas, A., Zhang J. and Behringer R. Buckling force chains in dense granular assemblies: physical and numerical experiments. *Geomechanics and Geoengineering: An International Journal* (2009)**4.1**: 3-16.

[21] Tordesillas, A, Walker D. M. and Lin, Q. Force cycles and force chains. *Phys. Rev. E* (2010)**81.1**: 011302.

[22] Liu, J., Nicot F. and Zhou W. Sustainability of internal structures during shear band forming in 2D granular materials. *Powder. Technol* (2018)**338**: 458-470.

[23] Cundall, P. A. and Strack, O. D. A discrete numerical model for granular assemblies. *Géotechnique* (1979) **29.1**: 47-65.

[24] Šmilauer, Václav, et al. "Using and programming." *The Yade Project, doi* 10 (2015).

[25] Peters, J. F., Muthuswamy, M., Wibowo, J. and Tordesillas, A. Characterization of force chains in granular material. *Phys. Rev. E* (2005)**72.4**: 041307.

[26] Kruyt, N. P. and Rothenburg, L. On micromechanical characteristics of the critical state of two-dimensional granular materials. *Acta. Mech* (2014) 225(8): 2301-2318.

[27] Kruyt, N.P. and Rothenburg, L. A micromechanical study of dilatancy of granular materials. *J. Mech. Phys. Solids* (2016)**95**: 411-427.

[28] Collins, I. F. and Muhunthan, B. On the relationship between stress–dilatancy, anisotropy, and plastic dissipation for granular materials. *Geotechnique* (2003)**53.7**: 611-618.

[29] Li, X. S. and Dafalias, Y. F. Dilatancy for cohesionless soils. *Geotechnique* (2000) **50.4**: 449-460.